Parameter Estimation of Cardiac Geometry by ECG-Gated PET Imaging: Validation Using Magnetic Resonance Imaging and Echocardiography

Gerold Porenta, William Kuhle, Shantanu Sinha, Janine Krivokapich, Johannes Czernin, Sanjiv S. Gambhir, Michael E. Phelps and Heinrich R. Schelbert

Division of Nuclear Medicine, Department of Molecular and Medical Pharmacology, University of California School of Medicine; and Laboratory of Structural Biology and Molecular Medicine, University of California, Los Angeles, California

The purpose of this study was to apply and validate a previously developed model-based image analysis technique which derives estimates of regional myocardial wall thickness and the left ventricular radius directly from gated cardiac PET images. **Methods:** In 11 normal volunteers, gated myocardial ^{18}F-deoxyglucose (FDG) images with 16 equal gates spanning the entire cardiac cycle were acquired for 20 min. To improve count statistics and thus image quality, 3 and 5 of 16 gates were summed to obtain systolic and diastolic images. Based on a five-parameter model, radial profiles from systolic and diastolic PET images were fit by nonlinear regression for myocardial wall thickness, left ventricular radius and tracer activities in the blood pool, the myocardial tissue and the extracardiac background. Echocardiography and gated magnetic resonance imaging (MRI) were performed in 11 and 7 volunteers, respectively. **Results:** We observed a significant ($p < 0.001$) correlation between measurements obtained by gated PET imaging and the correlative imaging modalities for myocardial wall thickness and left ventricular radius. While good agreement was observed between measurements of average radial shortening, estimates of average wall thickening differed significantly. **Conclusion:** This model-based analysis offers accurate estimates of regional recovery coefficients directly from gated cardiac PET images and may also prove useful for the assessment of myocardial contractile function. These recovery coefficients are essential for the correction of partial volume effects when quantitative PET studies are performed.

Key Words: positron emission tomography; tracer tissue quantification concentrations; partial volume effects; gated image acquisition

J Nucl Med 1995; 36:1123–1129

The limited spatial resolution of current PET images complicates or even precludes the extraction of true activity concentrations in myocardium directly from the acquired transaxial or reoriented images of the left ventricle. This is because of the partial volume effect (*1*) which becomes important when the size of the imaged object is less than twice the FWHM of the final image resolution. Commonly, values for the FWHM of cardiac PET images range from 8 to 15 mm depending on the reconstruction filter used. Given a normal myocardial wall thickness of about 10 mm, partial volume effects are important in cardiac imaging. The observed myocardial activity concentration generally underestimates the true activity concentration. However, partial volume effects are governed by a known, scanner-specific relationship between the size of the imaged object and the spatial resolution of the tomograph. Therefore, this underestimation of true tracer tissue activity concentrations can be corrected if the size and the shape of the imaged object is known or can be determined (*2–4*). The thickness of the left ventricular myocardium and the cavity dimensions can be determined readily and noninvasively with echocardiography. Echocardiographic images, however, are frequently difficult to align with the PET images so that echocardiographic measurements often do not correspond exactly or cannot be aligned accurately with the site of the PET tissue concentration measurements. Furthermore, it may be impossible to interrogate the entire left ventricle with echocardiography. Thus, the use of echocardiographic measurements may be limited for partial volume corrections or even may result in correction errors. Therefore, it would be desirable to determine the left ventricular dimensions directly from the PET images.

State-of-the-art PET scanners permit the acquisition of ECG-gated images. Therefore, parameters of cardiac geometry can be derived directly from PET images (*5*). As an additional advantage of gated image acquisition, the analysis of selected diastolic and systolic PET image frames

Received Jun. 22, 1994; revision accepted Jan. 3, 1995.

For correspondence and reprints contact: Heinrich R. Schelbert, MD, Dept. of Molecular and Medical Pharmacology, UCLA School of Medicine, Los Angeles, CA 90024-1735.

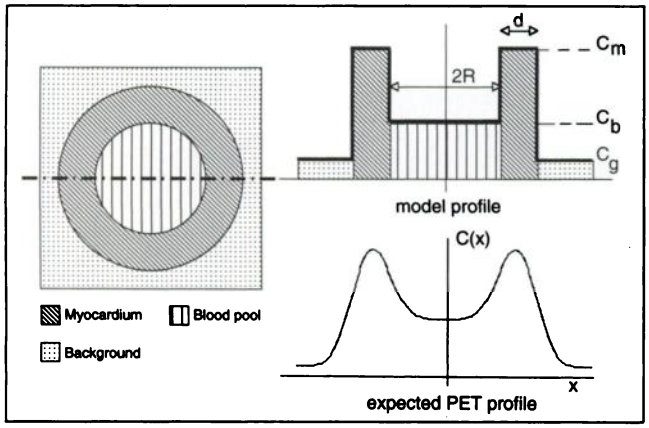

FIGURE 1. Schematic, two-dimensional model of the count activity distribution commonly depicted on a cardiac short-axis image (left panel). The right panel illustrates corresponding radial profiles through the center of the left ventricular cavity as expected in the ideal case (upper part) and as predicted by modeling PET images with a limited image resolution (lower part). The ideal count profile is specified by five parameters (C_b, C_m, C_g, R, d), while an additional parameter describing the PET scanner resolution (such as FWHM) is required to specify the PET profile (Eq. 1).

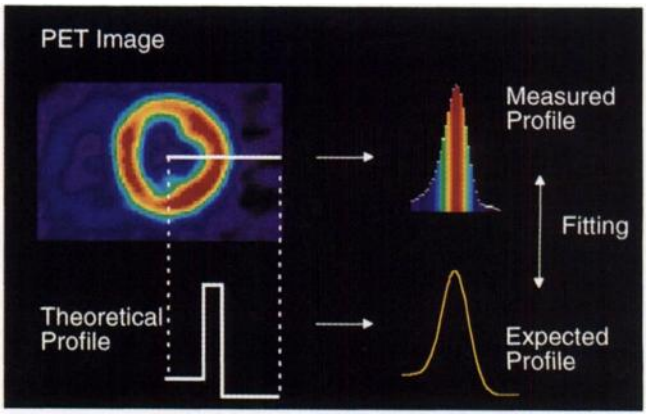

FIGURE 2. Example of model-based parameter estimation when applied to an ECG-gated diastolic short-axis PET image. The radial profile derived from the PET image is submitted to nonlinear regression analysis to obtain measurements of myocardial wall thickness and left ventricular radius.

might yield indices of regional myocardial contractile function, e.g., systolic radial shortening or wall thickening (*6*).

In the present study, we tested and validated a previously proposed model-based analysis technique (*3,4*) of gated PET images in order to derive estimates of myocardial wall thickness and the left ventricular radius during systole and diastole. In addition, we investigated whether measurements of myocardial wall thickening and radial shortening derived from gated PET images would offer quantitative indices of regional myocardial contractile function. The estimates derived from the PET images were compared against independent measurements by gated MRI and echocardiography.

MATERIALS AND METHODS

The Model

A simplified two-dimensional model of the count activity distributions commonly visualized on short-axis PET images of the left ventricle is composed of a circular blood pool surrounded by a concentric ring of homogeneous myocardial tracer activity and by extracardiac background activity (Fig. 1). The count activity profile obtained along a radial ray extending from the center of the left ventricle through myocardial tissue into the background can be directly obtained from this two-dimensional model.

As depicted in Figure 1, the radial count distribution is specified by five parameter values including the left ventricular radius R, the myocardial wall thickness d, the blood pool count activity C_b, the myocardial count activity C_m and the background activity C_g. From the theoretical model, the mathematical equation of a corresponding radial profile obtained from a PET image with limited image resolution can be derived by convolving the theoretical profile with the filter function of the PET scanning device (*3,4*). The equation of the tracer activity C(x) as a function of the radial excursion x originating from the center of the left ventricle (x = 0) is thus given by

$$C(x) = \frac{C_b}{2}\left(\mathrm{erf}\left(\frac{x+R}{s}\right) - \mathrm{erf}\left(\frac{x-R}{s}\right)\right) + \frac{C_m}{2}\left(\mathrm{erf}\left(\frac{x-R}{s}\right) - \mathrm{erf}\left(\frac{x-R-d}{s}\right) + \mathrm{erf}\left(\frac{x+R+d}{s}\right) - \mathrm{erf}\left(\frac{x+R}{s}\right)\right) + \frac{C_g}{2}\left(\mathrm{erf}\left(\frac{x-R-d}{s}\right) - \mathrm{erf}\left(\frac{x+R+d}{s}\right) + 2\right), \quad \text{Eq. 1}$$

where erf(u) is the error function

$$\mathrm{erf}(u) = \frac{2}{\sqrt{\pi}}\int_0^u e^{-t^2}\,dt, \quad \text{Eq. 2}$$

and

$$s = \frac{\mathrm{FWHM}}{2.355}. \quad \text{Eq. 3}$$

Based on this model, nonlinear regression analysis can be used to derive estimates for the five model parameters from reoriented PET short-axis images of the left ventricle (*3,4*). Because the tracer distribution on PET images is not symmetrical with respect to the LV center, Equation 1 was only fitted for values of $x \geq 0$ to radial rays originating from the center of the left ventricle and extending to an external end point as specified by an operator (Fig. 2). Thus, parameter values were independently obtained for each radial direction.

The simplified model of tracer activity distribution also assumes that radial count profiles can be modeled as a square wave function. This is why the model applies best to cardiac short-axis views. For transaxial images which frequently transsect the myocardial wall at an oblique rather than orthogonal angle, the model would be expected to provide less accurate estimates. Despite these theoretical constraints, we investigated whether the profile-fitting approach would also yield adequate estimates of cardiac geometry when applied to transaxial images.

PET Image Acquisition

After giving informed consent, 11 normal volunteers with a low probability of coronary artery disease (CAD) were studied with a

high-spatial resolution PET scanner (Model ECAT 931; CTI/Siemens, Knoxville, TN; 15 simultaneous image planes spaced 6.5 mm apart). A 20-min transmission scan was acquired to correct the emission images for photon attenuation. At the time of the transmission scan, 100 g of glucose (Trutol) were administered orally to enhance myocardial ^{18}F-deoxyglucose uptake and thus to increase the ratio of myocardial-to-background activity (*7*). Forty minutes after the intravenous injection of 10 mCi ^{18}F-deoxyglucose, gated image acquisition with 16 gates spanning the entire RR interval was performed for 20 min. The emission data were reconstructed into transaxial images (128 × 128-pixel matrix, 1.56 mm/pixel) on a dedicated minicomputer (microVAX, Digital Equipment Corporation, Maynard, MA) using a Shepp-Logan filter with a cutoff frequency of 0.48 cycles per centimeter yielding a final in-plane resolution of 10.5 mm FWHM. The axial resolution of the scanner was approximately 7 mm FWHM.

To improve count statistics, selected gates were summed to form a systolic and a diastolic image. By visual inspection of the gated image sequence, the image with the smallest left ventricular cavity and the thickest myocardial wall was identified and summed with the two directly adjacent images to obtain the systolic image. The average duration of the systolic image was 155 ± 21 msec. For the diastolic image, the last five gates occurring prior to and concurrent with the R-wave of the ECG signal were combined into a second summed image. The average duration of the diastolic image was 259 ± 35 msec.

PET Image Analysis

For further processing, the systolic and diastolic images were transferred to a low-cost desktop computer workstation (Macintosh IIci, Apple Computer Inc, Cupertino, CA). The transaxially acquired diastolic and systolic images were reoriented into short-axis views using image processing software as described previously (*8–10*). One pair of corresponding systolic and diastolic short-axis images located between the base of the heart and the insertion point of the papillary muscles was selected for further processing.

After an operator had drawn one circular region of interest (ROI) in the center of the left ventricular cavity and a second one outside of the epicardial border of the myocardium to encompass background activity, 60 equally spaced, radial profiles with a thickness of 1 pixel were generated from the center of the left ventricle to the outer boundary of the circular region. Nonlinear regression analysis was performed to fit the five-parameter model to each single profile. The effective FWHM value for each profile was calculated from the transaxial and the axial FWHM values and from the reorientation angle of the short-axis PET image as previously reported (*8*). On a Macintosh IIci computer with a 68030 processor clocked at 25 MHz, the average processing time to fit one radial profile was approximately 1.6 sec.

Individual values of both the internal radius and the wall thickness were combined using the associated chi-square values as weights to obtain average values for eight 45°-sectors as well as for the entire myocardium. Eighteen of 176 (10%) myocardial sectors which included part of the papillary muscle were excluded from this analysis to facilitate the comparison with echocardiography. The parameter estimation technique was applied also to a selected midventricular transaxial PET image. Similar to the analysis of reoriented images, a single, operator-defined center point was used to sector the entire transaxial image. The parameters derived by nonlinear regression analysis of the transaxial images were compared to those from gated magnetic resonance images.

Correlative Imaging Techniques

Two-dimensional and M-mode echocardiography were performed in all 11 volunteers with the transducer in the parasternal position. The left ventricular radius was measured from standard M-mode images in the parasternal long-axis view. For measurements of myocardial wall thickness, a complete cardiac cycle of two-dimensional short-axis images was digitized as a cine loop sequence (30 frames/sec) and analyzed using a semiautomated computer algorithm. Endocardial and epicardial borders were automatically generated by a computer algorithm and manually adjusted by the operator using a rubber band technique. Average values for myocardial wall thickness were derived for eight myocardial segments and for the entire myocardium.

MRI was performed in 7 of the 11 volunteers on a 0.3 T (12 MHz) Fonar Beta 3000-M scanner with a vertical field (Fonar, Melville, NY). The pulse sequence was optimized to obtain a multiplane and multigate acquisition protocol with flow compensated field echo images (256 phase encoding levels, 7-mm slice thickness, TE: 12 ms, TR: RR interval, 12–15 gates per heart cycle, flip angle 45°). No presaturation pulses were used since we worked with bright blood registration.

The location of the heart within the thoracic cavity was identified on coronal scout scans. Gated image sequences were then obtained spaced apart by 2 cm at 3 to 5 transaxial image levels encompassing the left ventricle. The image acquisition period required 60–90 min for completion. The MRI scanner model used in this study did not permit the use of double angulation techniques to obtain cardiac short-axis images. The number of transaxial image planes and their spacing was considered inadequate to reorient the acquired images into short-axis images. Thus, a gated transaxial image sequence obtained at a midventricular level was transferred to a Macintosh computer for further processing by medical image processing software (*9,10*).

After identification of systolic and diastolic MRI images by visual analysis of the image sequence, the operator outlined the center of the left ventricle and the endo- and epicardial borders on both images using a 256 × 256-pixel matrix with a pixel size of 1 × 1 mm. Automated computer software was then used to measure the left ventricular radius and the myocardial wall thickness along 64 equally spaced radial rays and to derive average values for eight 45° segments and for the entire left ventricle. Segments including parts of the mitral valve plane or of the papillary muscles were excluded from further analysis due to the low contrast between blood pool and myocardium that is frequently observed in these regions. A sample pair of systolic and diastolic PET and MRI images is depicted in Figure 3.

RESULTS

Measurements of mean myocardial wall thickness and mean left ventricular radius derived from reoriented gated PET images and from echocardiographic images in 11 normal volunteers are compared in Figure 4. A significant correlation was observed between the two imaging modalities for both wall thickness measurements (PET-d = 0.49 Echo-d + 7.2, s.e.e. = 0.067, r = 0.87, n = 22) and measurements of left ventricular radius (PET-r = 0.84 Echo-r + 1.7, s.e.e. = 0.11, r = 0.87, n = 22). However, the slope of the regression line for wall thickness values

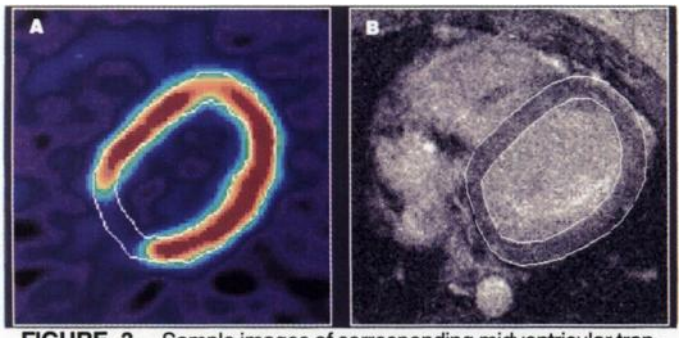

FIGURE 3. Sample images of corresponding midventricular transaxial views acquired during cardiac diastole with gated PET imaging (A) and gated MR imaging (B). Regions of interest delineating the endocardial and epicardial borders are displayed as graphical overlays in white.

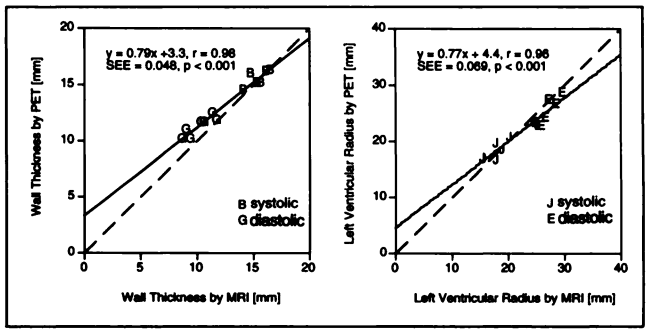

FIGURE 5. Regression plots between the average myocardial wall thickness (A) and left ventricular radius (B) as derived from transaxial images by magnetic resonance and PET imaging. The dashed line indicates the line of identity for reference purposes.

was lower than the corresponding slope for values of the left ventricular radius due to a systematic overestimation of the diastolic wall thickness by PET measurements.

When segmental rather than average values of myocardial wall thickness were compared, the equation of the regression line was essentially unchanged while the observed correlation coefficient was reduced (PET-d = 0.45 Echo-d + 7.6, s.e.e. = 0.053, r = 0.56, n = 158). This increased data scatter probably reflects inaccuracies in aligning myocardial segments between the reoriented PET images and the two-dimensional short-axis echo images. As echocardiographic measurements of the left ventricular radius were not obtained from the two-dimensional images but from the more precise M-mode imaging technique, a regression analysis by segments could not be performed for segmental values of the left ventricular radius.

Figure 5 depicts the results of regression analysis comparing PET and MRI measurements of cardiac dimensions derived from transaxial images at a midventricular level. Based on theoretical considerations, the profile-fitting method is not entirely adequate for the analysis of transaxial PET images, but the correlation of measurements between both imaging modalities was highly significant (PET-d = 0.79 MRI-d + 3.3, s.e.e. = 0.048, r = 0.98, n = 13; PET-r = 0.77 MRI-r + 4.4, s.e.e. = 0.069, r = 0.96, n = 13). The use of midventricular cross sections which are oriented relatively perpendicular to the image plane most likely accounts for the good agreement.

When individual segmental rather than average values were correlated, the results of the regression analysis closely mirrored the results obtained by comparing average values (PET-d = 0.85 MRI-d + 2.5, s.e.e. = 0.072, r = 0.82, n = 69; PET-r = 0.8 MRI-r + 3.7, s.e.e. = 0.05, r = 0.89, n = 69). Table 1 summarizes the different results obtained by regression analysis.

Fractional shortening of the left ventricular diameter and myocardial wall thickening have been used successfully as quantitative descriptors of regional myocardial wall motion. Thus, we also studied the feasibility to assess regional contractile function based on estimates from our model-fitting approach by comparing the measurements of relative radial shortening and relative wall thickening obtained from echo and gated PET images (Fig. 6). Measurements of mean fractional radial shortening derived from PET (30% ± 4%) and echo (31% ± 9%) images were not significantly different (p = n.s., paired t-test, n = 11). However, the measurements of wall thickening assessed by PET

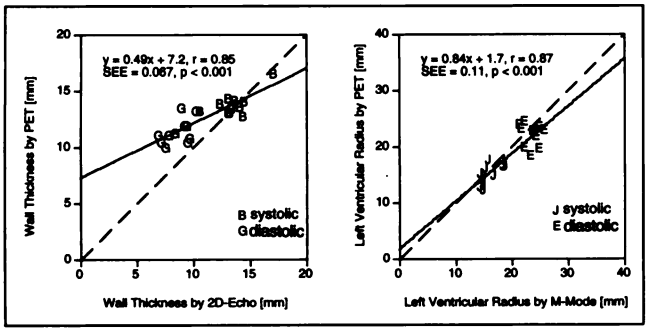

FIGURE 4. Regression plots between the average myocardial wall thickness (A) and the left ventricular radius (B) as derived from short-axis images by echocardiography and PET imaging. The dashed line indicates the line of identity for reference purposes.

TABLE 1
Results of Regression Analysis

	r	Slope	s.e.e.	Intercept	n
Wall thickness					
2D-Echo (avg.)	0.85	0.49	0.067	7.2	22
2D-Echo (seg.)	0.56	0.45	0.053	7.6	158
MRI (avg.)	0.98	0.79	0.048	3.3	13*
MRI (seg.)	0.82	0.85	0.072	2.5	69
LV radius					
M-Mode	0.87	0.84	0.110	1.7	22
MRI (avg.)	0.96	0.77	0.069	4.4	13*
MRI (seg.)	0.89	0.80	0.050	3.7	69

*In one volunteer, a low image quality of the systolic magnetic resonance image precluded the contouring of the endo- and epicardial borders so that the image had to be omitted from further analysis.

avg. = average value for each patient; r = correlation coefficient; s.e.e. = standard error of the estimate; and n = number of points.

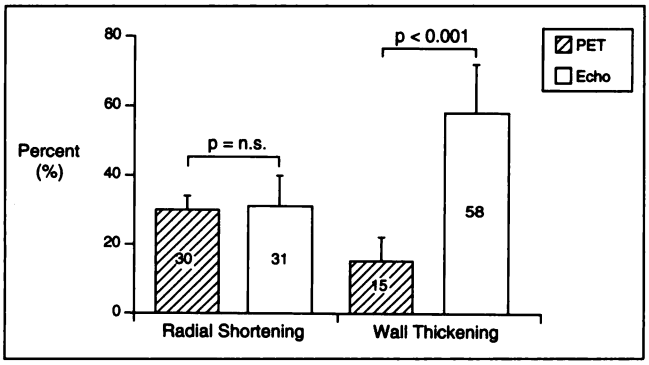

FIGURE 6. Fractional radial shortening and myocardial wall thickening from diastole to systole as obtained from echocardiographic and PET images. Statistical analysis showed a significant difference for the average segmental wall thickening between PET and echocardiography (paired t-test, $p < 0.001$).

(15% ± 7%) were significantly lower than values from echo (58% ± 14%) due to the overestimation of diastolic wall thickness values by the model-fitting method ($p < 0.001$, paired t-test, $n = 11$).

A statistical analysis of the fractional radial shortening in eight anatomical segments revealed a significant difference between segments ($p < 0.001$, ANOVA). Therefore, we compiled a normal database of mean values (μ) and standard deviations (s.d.) for the regional radial shortening fraction and displayed the normal range between $\mu + 2$ s.d. and $\mu - 2$ s.d. using a polar coordinate system (Fig. 7). When patient data are plotted within this display frame, a graphical representation is obtained that provides a simple interpretation and quantitative assessment of the regional myocardial wall motion.

To assess the impact of applying the model-fitting algorithm to systolic rather than ungated images, we also tested whether the profile-fitting algorithm would provide adequate correction values when applied to ungated images.

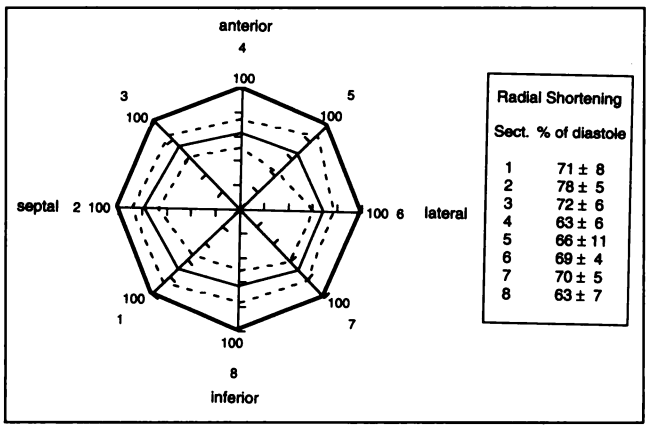

FIGURE 7. Polar map plot of the fractional shortening of the left ventricular radius between diastole (100%) and systole (% of diastolic value) for eight myocardial segments (plot: normal range = mean ± 2 s.d.; table: values as mean ± s.d.). Statistical analysis revealed a significant difference between the segmental values (ANOVA, $p < 0.001$).

While this approach, however, would not require gated image acquisition and thus be more convenient to implement, we found that corrected activity values derived from ungated images are 17% ± 13% lower than the corresponding values obtained from systolic gated images taken as a reference standard. This difference was significantly different from 0 (t-test, $p < 0.001$) and probably precludes the use of ungated images for the correction of partial volume and wall motion effects by the proposed algorithm.

DISCUSSION

This study employed model-based parameter estimation techniques to derive from gated cardiac FDG images systolic and diastolic measurements of regional myocardial wall thickness and left ventricular radius in normal subjects. We found a significant correlation between these measurements and corresponding values obtained from two correlative imaging techniques, echocardiography and gated MRI. It should be noted, however, that systolic and diastolic measurements are clustered into two data groups so that correlation analysis may partly reflect the distribution of the measurements.

For measurements of diastolic wall thickness, we found a systematic overestimation by the model-based estimation technique when compared to echocardiography and MRI. This overestimation can partly be attributed to wall motion effects that are expected to be more pronounced for the diastolic PET image with an average duration of 269 msec as compared to the echocardiographic image with a duration of 33 msec even though wall motion during diastolic diastasis is expected to be limited. Also, the performance of the model-fitting approach is expected to depend on the image resolution and object size and probably degrades for objects that are significantly smaller than the FWHM value such as the normal diastolic myocardium.

Parameters derived through our model-fitting technique can also be used to characterize and assess regional myocardial contractile function. While myocardial wall thickening cannot be tracked with sufficient accuracy based on our method, the regional fractional shortening of the left ventricular radius can be reliably delineated. Similar to previous investigations that used echocardiographic imaging or ultrafast computed tomography (*11–13*), we also observed a significant difference in radial shortening fractions between different anatomical segments. Therefore, the interpretation of results obtained from patient studies should be performed with respect to the variations observed in a group of normal subjects.

The estimation technique proposed in the present study could prove useful to eliminate or lessen artifactual inhomogeneities of the regional tissue tracer activity due to partial volume and wall motion effects. Moreover, this method may also be used to derive corrected time-activity curves for tracer kinetic models from dynamic image sequences. Currently, dynamic image acquisition still precludes a simultaneous gated acquisition mode. If, however,

gated images are acquired subsequent to the dynamic acquisition period, the true tracer tissue concentrations can be estimated from the systolic portion of these images by a model-based analysis. These estimates are expected to be accurate because artifacts associated with wall motion or partial volume effects would be reduced and because the accuracy of the model-fitting technique is better for systolic images as has been shown in the present study. The ratio between estimates of the true tracer tissue activities and corresponding uncorrected activity values from ungated images could be applied as correction factors to the time-activity curves from dynamic images to correct for wall motion and partial volume effects.

In certain circumstances, the particular biodistribution of tracer substances permits the use of simplified graphic methods to derive quantitative estimates of kinetic parameters of potential clinical relevance (*14*). For these methods, partial volume correction is intrinsic to the model specifications and need not be done explicitly. However, while these methods provide quantitative cardiac PET imaging, they apply only in selected cases and do not offer a noninvasive assessment of regional contractile function.

Previous studies have attempted to utilize the observed change of myocardial count activities from systolic to diastolic time frames to assess myocardial contractility (*6,15*). While this simple method may be useful to study regional patterns of myocardial contractility, it does not provide quantitative estimates of regional myocardial wall thickness or left ventricular radius and thus does not allow the implementation of automated algorithms for partial volume correction.

Our model-based estimation technique of cardiac geometry, however, is also associated with several limitations. Firstly, an ECG-gated acquisition mode requires that a stable and regular cardiac rhythm be maintained throughout the acquisition period which may not be fulfilled in patients with heartbeat irregularities such as atrial fibrillation or extrasystole. Moreover, successful profile fitting also requires that the gated images be of high image quality with adequate count rates. Therefore, when compared to acquisition protocols for static PET imaging, the acquisition time for gated PET imaging needs to be increased or a higher dose of tracer activities needs to be administered. Both these adjustments to the imaging protocol may not always be feasible either in patients or in PET studies that involve several sequential injections of tracer substances. Lastly, in myocardial segments with reduced or absent tracer uptake, the fitting algorithm may fail and thus will be of limited value. It remains to be determined, however, how the fitting algorithms will perform in myocardial segments with a moderate decrease in count activity or with an uneven tracer distribution.

CONCLUSION

A previously developed, model-based parameter estimation technique has been validated. The approach offers estimates of regional cardiac dimensions during systole and diastole and can be derived directly from gated PET images. The approach should prove useful for correction of partial volume and wall motion effects and, thus, for quantitative PET imaging. Moreover, the method offers a unique possibility to relate noninvasively and near simultaneously regional myocardial perfusion, metabolism and contractile function.

ACKNOWLEDGMENTS

The authors thank Ron Sumida, Francine Aguilar, Judy Edwards, Anne Irwin and Gloria Stocks for their excellent technical assistance; the staff of the Medical Cyclotron at UCLA for providing the isotopes; and Eileen Rosenfeld for her skillful secretarial assistance.

The Laboratory of Structural Biology and Molecular Medicine is operated for the U.S. Department of Energy by the University of California under Contract #DE-FC03-87ER60615. This work was supported in part by the Director of the Office of Energy Research, Office of Health and Environmental Research, Washington, D.C., by Research Grants #HL 29845 and #HL 33177, National Institutes of Health, Bethesda, MD; and by an Investigative Group Award by the Greater Los Angeles Affiliate of the American Heart Association, Los Angeles, CA. William Kuhle is the recipient of an American Heart Association Medical Student Research Fellowship and Dr. Gambhir is a member of the UCLA Crump Institute for Biological Imaging.

REFERENCES

1. Hoffman EJ, Huang SC, Phelps ME. Quantitation in positron emission computed tomography: 1. Effect of object size. *J Comput Assist Tomogr* 1979;3:299–308.
2. Henze E, Huang SC, Ratib O, Hoffman EJ, Phelps ME, Schelbert HR. Measurements of regional tissue and blood-pool radiotracer concentrations from serial tomographic images of the heart. *J Nucl Med* 1983;24: 987–996.
3. Gambhir SS. Quantitation of the physical factors affecting the tracer kinetic modeling of cardiac positron emission tomography data, PhD Thesis. University of California, Los Angeles, 1990.
4. Gambhir SS, Huang, SC, Phelps ME. New mathematical methods for the correction of resolution effects and for geometrical parameter estimation in cardiac PET studies. *Phys Med Biol* 1995:in press.
5. Hoffman EJ, Phelps ME, Wisenberg G, Schelbert HR, Kuhl DE. Electrocardiographic gating in positron emission computed tomography. *J Comput Assist Tomogr* 1979;3:733–739.
6. Yamashita K, Tamaki N, Yonekura Y, et al. Quantitative analysis of regional wall motion by gated myocardial positron emission tomography: validation and comparison with left ventriculography. *J Nucl Med* 1989;30: 1775–1786.
7. Berry JJ, Baker JA, Pieper KS, Hanson MW, Hoffman JM, Coleman RE. The effect of metabolic milieu on cardiac PET imaging using fluorine-18-deoxyglucose and nitrogen-13-ammonia in normal volunteers. *J Nucl Med* 1991;32:1518–1525.
8. Kuhle W, Porenta G, Huang S, Phelps M, Schelbert H. Issues in the quantitation of reoriented cardiac PET images. *J Nucl Med* 1992;33:1235–1242.
9. Ratib O, Huang HK. CALIPSO: an interactive software package for multimodality medical image analysis on a personal computer. *J Med Imaging* 1989;3:205–216.
10. Porenta G, Kuhle W, Czernin J, Ratib O, Brunken RC, Schelbert HR. Interactive user-friendly image analysis of cardiac PET images on a low cost desktop computer. In: *Computers in cardiology*. Los Alamitos, CA: IEEE Computer Society Press; 1991:245–248.
11. Haendchen RV, Wyatt HL, Maurer G, et al. Quantitation of regional cardiac function by two-dimensional echocardiography: I. Patterns of contraction in the normal left ventricle. *Circulation* 1983;67:1234–1245.
12. Pandian NG, Skorton DJ, Collins SM, Falsetti HL, Burke ER, Kerber RE.

Heterogeneity of left ventricular segmental wall thickening and excursion in 2-dimensional echocardiograms of normal human subjects. *Am J Cardiol* 1983;51:1667–1673.

13. Feiring AJ, Rumberger JA, Reiter SJ, Collins SM, Skorton DJ, Rees M, Marcus ML. Sectional and segmental variability of left ventricular function: experimental and clinical studies using ultrafast computed tomography. *J Am Coll Cardiol* 1988;12:415–425.
14. Choi Y, Hawkins RA, Huang SC, et al. Parametric images of myocardial metabolic rate of glucose generated from dynamic cardiac PET and 2-F fluoro-2-deoxy-d-glucose studies. *J Nucl Med* 1991;32:733–738.
15. Yamashita K, Tamaki N, Yonekura Y, et al. Regional wall thickening of left ventricle evaluated by gated positron emission tomography in relation to myocardial perfusion and glucose metabolism. *J Nucl Med* 1991;32:679–685.